Thermogravimetric analysis and kinetic modeling for empty fruit bunch date palm pyrolysis

Casimir Kalibé Fanezouné [a,*], Asma Dhahak [b], Jorge Peixinho [b], Hassan El Bari [a]

[a] SETIME Laboratory, Faculty of Sciences, Ibn Tofail University, BP 133, Kénitra, Morocco
[b] Laboratoire PIMM, CNRS Arts et Métiers Institute of Technology, Cnam, HESAM Université, 75013 Paris, France

ARTICLE INFO

Keywords:
Thermogravimetric analysis
Kinetic modeling
Pyrolysis
Shrinkage
Activation energy

ABSTRACT

This study presents a comparative analysis of different kinetic models applied to the thermochemical pyrolysis of palm empty fruit bunch (PEFB). The kinetic parameters, particularly the activation energy, are determined through thermogravimetric analysis (TGA) of samples that underwent heating rates ranging from 10 to 50 °C/min. Image analysis of PEFB in a hot-stage microscope reveals an intriguing correlation between the observed shrinkage and the conversion rate (α) and indicates that significant physical and chemical transformations occurred within α between 0.2 and 0.8. The experimental data from TGA demonstrates good alignment with four distinct kinetic models. The Coast-Redfern model gives activation energies ranging from 60 to 134 kJ/mol for α between 0.2 and 0.8. In contrast, the Kissinger model and the isoconversion models, Kissinger-Akahira-Sunose and Ozawa-Flyn-Wall, show higher activation energy of 151, 156, and 157 kJ/mol, respectively. The findings underscore the significant impact of the selected kinetic model on determining kinetic parameters.

1. Introduction

Global warming, caused by the emission of greenhouse gases, is an urgent issue. Second-generation biomass made up of residues and organic waste (Rousset, 2013; Beniche et al., 2021; Sounni et al., 2023; Habchi et al., 2024), such as date palm empty fruit bunch (PEFB), offers a promising alternative, both economically and environmentally, for reducing the demand for fossil fuels to meet the world's need for transport fuel and certain basic chemical products (Ouhammou et al., 2019; El Gnaoui et al., 2022; Ouhammou et al., 2022).

According to the Moroccan Ministry of Agriculture (Sedra, 2015), the date palm sector in Morocco spans over 59,600 ha. Recent studies by Agoudjil et al., (2011) and Ghnimi et al., (2017) reveal a potential for over 2 million tons of waste from the exploitation of >200 million date palms globally.

PEFB, in particular, is known to be composed of significant amounts of cellulose, hemicellulose, and lignin, making it a valuable feedstock for energy recovery through thermochemical conversion methods like pyrolysis (Nasser et al., 2016; Raza et al., 2021; Lahboubi et al., 2022a; Akinnawo et al., 2023).

Pyrolysis is a thermochemical process that converts biomass or plastic waste into fuel in a deoxygenated environment, using high temperatures and specific heating rates (El Bari et al., 2024; Liang et al., 2024). The pyrolysis of lignocellulosic biomass, such as PEFB, has several advantages, as it produces green energy that is environmentally friendly, not time-consuming, and increasingly economically competitive with fossil fuels (Bensidhom et al., 2018). The pyrolysis of PEFB results in the production of three products: bio-oil, biochar and a gas. These products have the potential to be utilized in a variety of applications, including the production of biofuels, chemicals and energy. This represents a promising method for converting agricultural waste into valuable products, there by promoting the management of waste and the production of renewable energy. In fact, the maximum yield of bio-oil is typically around 40–45%wt, obtained at pyrolysis temperatures of 450–500 °C (Sutrisno and Hidayat, 2018; Nzihou et al., 2019; Al-Maari et al., 2021). Bio-oil is a complex mixture of compounds, including acids, aldehydes, ketones, alcohols, phenols, and oligomers. Ferreira et al., (2020) identified the main compounds present in the bio-oil as hexadecenoic acid methyl ester, nonane, hexadecenoic acid, and phenol. The bio-oil displays a high antioxidant capacity due to the phenolic compounds. Al-Maari et al., (2021) observed that the pyrolysis of PEFB qualitatively yielded 44.37 % esters, 5.09 % phenols, 5 % carbonyls, 23.7 % acids, and 15.85 % hydrocarbons. The biochar yield is typically 25–30%wt and exhibits characteristics similar to sub-bituminous coal,

* Corresponding author.
E-mail address: casimir.kalibefanezoune@uit.ac.ma (C.K. Fanezouné).

with a calorific value of approximately 5000 kcal/kg (Handoko et al., 2021; Ferreira et al., 2020; Makowska and Dziosa, 2024). The biochar can be used in numerous fields, such as renewable fuel, metallurgy, leisure industries, soil amendment, activated carbon, and electrode production (Ferreira et al., 2020). The gas is a syngas, which is a mixture of methane (13–17 %), hydrogen (28–33 %), carbon monoxide (17–26 %), and carbon dioxide (16–31 %) (Handoko et al., 2021). The calorific value of syngas ranges from 2600 to 3300 kcal/Nm^3, and it can be employed as an energy source for the pyrolysis process itself or as a feedstock for chemical synthesis, such as methanol (Handoko et al., 2021).

The yields and compositions of the products depend on the pyrolysis conditions, including temperature, heating rate, and residence time. In order to ensure the effective and optimal utilization of PEFB as a raw material, it is essential to gain a thorough comprehension of the interrelationship between these parameters, the pyrolysis process and its associated kinetics.

Various kinetic models, including Ozawa-Flynn-Wall (OFW), Kissinger-Akahira-Sunose (KAS) and Friedman have been used to analyze the pyrolysis of PEFB. For instance, Fauziyah et al., (2024) found activation energy values between 50.9 and 169.6 kJ/mol at heating rates (β) of 5, 10, and 20 °C/min using methods such as Friedman, KAS, OFW, and Starink. Conversely, the study of Raza et al., (2021) found activation energies ranging from 96 to 114 kJ/mol using the Coast Redfern approach under similar heating conditions at a single heating rate of 10 °C/min. In addition, Nyakuma B.B. et al., (2015) used the OFW model over these three heating rates and found an average activation energy of 160 kJ/mol.

However, it is rare to find studies in the literature that analyze the kinetics of PEFB specifically at heating rates of up to 50 °C/min and compare the efficiency of the different models used.

In this context, and in order to provide a more comprehensive insight into the pyrolysis process, especially at different and higher heating rates, this study aimed to reveal new perspectives on the kinetic and morphological evolution of PEFB. The investigation began by studying the behavior of PEFB using thermogravimetric analysis (TGA) at five different heating rates. The thermal behaviors, the shrinkage, the color changes, and the morphological evolution during PEFB pyrolysis were then observed using a hot stage microscope. Continuous monitoring of shrinkage with increasing temperature provided good insights into the physical and chemical changes of the PEFB. The research also included an analysis of the kinetic model for PEFB pyrolysis. This involved determining the activation energies and pre-exponential factor and comparing the effectiveness of different models: Kissinger (Blaine and Kissinger, 2012), Coats-Redfern (CR) (Ke et al., 2011), and Ozawa-Flynn-Wall (OFW) (Phuakpunk et al., 2020). The strengths and limitations of each model were evaluated in detail. The Kissinger-Akahira-Sunose (KAS) isoconversion models were used in addition to the OFW isoconversion method.

The results of this study can help fine-tune the necessary characteristics of the pyrolysis reactor for this biomass and guide the selection of influential parameters to optimize the yield and quality of the pyrolysis products.

2. Materials and methods

2.1. Biomass: sample preparation and characterization

PEFB came from date palms in south-east of Morocco (Draa-Tafilalet). A blinder was used to reduce the size of the substrate (size <5 mm). Before being used, the substrate was kept at 5 °C. The total solid was determined by drying the sample for 24 h at 105 °C. The method DIN 51732: 2014–07:L was used to carry out the ultimate analysis to determine the composition of carbon, oxygen, nitrogen, and hydrogen. Fiber contents (acidic detergent fiber, neutral detergent fiber, and acid detergent lignin) were analyzed using a Gerhard Fibretherm cellulose extractor, following the Weender method and the van Soest detergent analysis method (Strauch et al., 2018). The fiber content allows hemicelluloses, cellulose, and lignin compositions to be determined (Elsayed et al., 2018).

2.2. Experimental methods

2.2.1. Thermogravimetric analysis (TGA)

TGA was performed using a TA Instrument Q500. The sample, weighing between 6 and 8 mg and cut into small pieces, underwent heating rates of 10, 20, 30, 40, and 50 °C/min under a nitrogen flow rate of 90 mL/min until the final temperature of 600 °C. The analysis was conducted in a 100 µL platinum crucible.

2.2.2. Visualization of PEFB through hot stage microscope

A hot-stage microscope, allowing for the observation and analysis of morphological transformations of PEFB materials experiencing controlled temperature variation is used. This tool allows for the monitoring of the biomass as it changes with time and temperature. During the process, the sample was placed between two thin glass slides in the hot-stage micro-reactor (Linkam cell THMS600) and positioned under a Nikon optical microscope. To create an inert environment, liquid nitrogen was used. The sample was then rapidly heated to 500 °C at a rate of 150 °C/min using control software. A 22 mm diameter heating plate with a 2 mm quartz disk served as the base for the sample. The sample was observed using transmitted light captured from above at 5× magnification while being heated. A color video camera with a resolution of 1200 × 1600 pixels was used to capture images based on temperature and time (Dhahak et al., 2024).

From these images, the shrinkage ratio, S, is defined based on the area by:

$$S = 100 \times \frac{A_0 - A(t)}{A_0} \quad (1)$$

Where A(t) is the area at instantaneous time t and A_0 is the initial area of the sample PEFB.

2.3. Modeling of kinetics

Kinetic analysis techniques can be categorized into two main categories: model fitting and isoconversion methods. Model fitting involves identifying reaction kinetic model phenomena, while isoconversion methods are used to determine the activation energy of a reaction at different conversion levels (Soon et al., 2016).

In this study, intrinsic reaction rate coefficients for the pyrolysis of PEFB under different heating rates are determined to Eq. (2) (Ahmad et al., 2017) as follows:

$$\frac{d\alpha}{dt} = k(T) f(\alpha) \# \quad (2)$$

Where t is the time, $k(T)$ is the constant depending on the temperature T, and $f(\alpha)$ is the reaction model and shows the relationship between the reaction rate and the evolution of the conversion rate, α, given by:

$$\alpha = \frac{m_i - m_T}{m_i - m_f} \# \quad (3)$$

where m_i, m_T and m_f are, respectively, the initial mass, mass at temperature T and final mass of the sample.

The relationship between temperature and rate constants is defined by the Arrhenius equation, formulated as follows:

$$k(T) = A \times exp\left(-\frac{E_a}{RT} \right) \quad (4)$$

Where E_a is the activation energy, the ideal gas constant is R =

8.3145 J.mol^{-1}.K^{-1} and the pre-exponential factor is A.

The pre-exponential factor A, also known as the frequency factor, indicates the rate at which molecules collide during a reaction. Consequently, it provides the frequency of molecular collisions with the proper particle orientation and temperature for the reaction to proceed.

The primary kinetic model function utilized for biomass pyrolysis, as proposed by (Gil et al., 2010; Xie et al., 2018; Matali et al., 2020) is given by:

$$f(\alpha) = (1-\alpha)^n \# \tag{5}$$

Where n is the kinetic order of the reaction.

By incorporating Eq. (2), (4), and (5), a new equation can be derived.

$$d\alpha \Big/ dt = A \times exp\left(-\frac{E_a}{RT}\right) \times (1-\alpha)^n \# \tag{6}$$

Due to the dynamic nature of the data, samples are acquired at a constant heating rate ($\beta = dT/dt = $ constant), this is integrated into Eq. (6). As a result, the rate expression can be reformulated into a non-isothermal rate expression that characterizes the reaction as a function of temperature at a constant rate, as follows:

$$\frac{d\alpha}{dT} = \frac{A}{\beta} \times exp\left(-\frac{E_a}{RT}\right) \times (1-\alpha)^n \# \tag{7}$$

After rearrangement, the equation can be expressed as:

$$\frac{d\alpha}{(1-\alpha)^n} = \frac{A}{\beta} \times exp\left(-\frac{E_a}{RT}\right) dT$$

Introducing the function $g(\alpha) = \int_0^\alpha \frac{d\alpha}{(1-\alpha)^n}$, we obtain:

$$g(\alpha) = \int_0^\alpha \frac{d\alpha}{(1-\alpha)^n} = \int_{T_i}^{T_f} \frac{A}{\beta} \times exp\left(-\frac{E_a}{RT}\right) dT \# \tag{8}$$

It is important to highlight that for biomass pyrolysis, it is common to assume a first-order reaction ($n = 1$) as the kinetic model (Anca-Couce et al., 2014; Fauziyah et al., 2024). However, the present study aims to take a more comprehensive approach by investigating the reaction orders at $n = 1$, 1.5, and 2. Studying these different reaction orders allows the determination of the most appropriate order that best describes PEFB pyrolysis process.

2.3.1. Model-free kinetics: coats and Redfern approximation

This is a fitting method based on optimization of the reaction order, A and E_a. This approach is thoroughly explained in the literature (Naqvi et al., 2019; Boukaous et al., 2021; Sidek et al., 2022). But in this instance, as previously said, the first order was already considered for biomass pyrolysis. This method is sensitive to measurement noise and requires the results to be as accurate as possible.

The Coats and Redfern (CR) method can be derived from Eq. (8). For a first-order reaction where $n = 1$, the primary kinetic model function leads to:

$$f(\alpha) = 1 - \alpha$$

Then

$$g(\alpha) = -ln(1-\alpha) = \int_0^\alpha \frac{d\alpha}{1-\alpha} = \int_{T_i}^{T_f} \frac{1}{\beta}\left[A \times exp\left(-\frac{E_a}{RT}\right)\right] dT \# \tag{9}$$

After integration, we obtain for $T_i = T_0 = 0$ and $T_f = T$:

$$ln\left[-\frac{ln(1-\alpha)}{T^2}\right] = ln\frac{AR}{\beta E_a} - \frac{E_a}{RT}\#$$

For $n = 1.5$, Eq. (4) leads to:

$$f(\alpha) = (1-\alpha)^{1.5}$$

Then

$$g(\alpha) = -ln(1-\alpha)^{1.5} = \int_0^\alpha \frac{d\alpha}{(1-\alpha)^{1.5}} = \int_{T_i}^{T_f} \frac{1}{\beta}\left[A \times exp\left(-\frac{E_a}{RT}\right)\right] dT$$

After integration, for $T_i = T_0 = 0$ and $T_f = T$, we obtain:

$$ln\left\{\frac{2\left[(1-\alpha)^{1.5} - 1\right]}{T^2}\right\} = ln\left[\frac{AR}{\beta E_a}\left(1 - \frac{2AR}{\beta E_a}\right)\right] - \frac{E_a}{RT}\# \tag{10}$$

$$ln\left\{\frac{2\left[(1-\alpha)^{1.5} - 1\right]}{T^2}\right\} = ln\,\frac{AR}{\beta E_a} - \frac{E_a}{RT}$$

For second order $n = 2$, Eq. (5) leads to:

$$f(\alpha) = (1-\alpha)^2$$

Then,

$$g(\alpha) = -ln(1-\alpha)^2 = \int_0^\alpha \frac{d\alpha}{(1-\alpha)^2} = \int_{T_i}^{T_f} \frac{1}{\beta}\left[A \times exp\left(-\frac{E_a}{RT}\right)\right] dT$$

After integration, we obtain, for $T_i = T_0 = 0$ and $T_f = T$:

$$ln\left\{\frac{[1/(1-\alpha)] - 1}{T^2}\right\} = ln\left[\frac{AR}{\beta E_a}\left(1 - \frac{2AR}{\beta E_a}\right)\right] - \frac{E_a}{RT}$$

$$ln\left\{\frac{[1/(1-\alpha)] - 1}{T^2}\right\} = ln\frac{AR}{\beta E_a} - \frac{E_a}{RT}\# \tag{11}$$

plotting $ln\left[-\frac{ln(1-\alpha)}{T^2}\right]$, $ln\left\{\frac{2\left[(1-\alpha)^{1.5}-1\right]}{T^2}\right\}$ and $ln\left\{\frac{[1/(1-\alpha)]-1}{T^2}\right\}$ as a function of $1/T$, respectively, $n = 1$, $n = 1.5$, and $n = 2$, yields a linear relationship with a slope of E_a/R. Eq. (9) is solved between $[T_i; T_f]$ for the five heating rates. The term $\frac{2AR}{\beta E_a}$ is often disregarded in the literature. Based on various heating rates, average values for the parameters E_a and A are determined.

2.3.2. Kissinger method

Kissinger's method is widely used in the analysis of solids and the decomposition of liquids under non-isothermal conditions. Developed by Kissinger, this model-free approach offers a means to determine the activation energy (E_a) of a system by examining the variation of the maximum temperature of the exothermic peak T_m as a function of the heating rate.

The pyrolysis reaction is regarded as a single reaction for biomass degradation, generating bio-oil, gas, and bio-char. The Kissinger relationship can be simplified as follows:

$$ln\left(\frac{\beta}{T_m^2}\right) = ln\left(\frac{AR}{E_a}\right) - \frac{E_a}{RT_m}\# \tag{12}$$

where T_m is the maximum temperature of the $\frac{d\alpha}{dt}$ curve associated with the maximum reaction rate, and β is the heating rate.

This method allows the activation energy value to be obtained from the slope $ln\left(\frac{\beta}{T_m^2}\right)$ as a function of $1/T$ for a series of experiments at different heating rates, β.

2.3.3. Iso-conversional modeling of TGA results: Kissinger-Akahira-Sunose method (KAS) and Ozawa- Flynn-Wall method (OFW)

2.3.3.1. Ozawa- Flynn-Wall (OFW) method. The OFW method is one of the linear integral methods and is derived from the Doyle approximation (Zhong et al., 2024). It is formulated by the following equation:

$$ln\beta = ln\left[\frac{AE_a}{Rg(\alpha)}\right] - 5.335 - 1.0516\left(\frac{E_a}{RT}\right)\# \quad (13)$$

It is used to obtain the apparent activation energy E_a from a natural log plot of heating rates, ln β, as a function of $1/T$, which represents the linear relationship with a given conversion value at different heating rates.

2.3.3.2. Kissinger-Akahira-Sunose method (KAS). Iso-conversion methods are widely used to study kinetic parameters. The KAS method, inspired by the Kissinger method, is reputed to be excellent for managing the complexity of the biomass decomposition reaction, unlike the Coats-Redfern method. KAS is based on the assumption that, when the value of the reaction rate is constant, the activation energy is a function of temperature only. These temperatures are given experimentally for this study at 10, 20, 30, 40, and 50 °C/min.

Following the integration and reorganization of (5), the KAS method can be expressed as follows:

$$ln\left(\frac{\beta_i}{T_\alpha^2}\right) = ln\left[\frac{A_\alpha R}{E_\alpha g(\alpha)}\right] - \frac{E_\alpha}{RT_\alpha} \quad (14)$$

Where g is a complex integral function. Plotting $ln\left(\frac{\beta_i}{T_\alpha^2}\right)$ is as a function of $\frac{1}{T}$. The integral reaction mechanism $g(\alpha)$ indicates that the limiting step of the reaction is chosen on the basis of the best-fit data with the correlation coefficient, R^2 close to one.

The activation energy (Ea) and pre-exponential factor (A) were determined through the application of the Kissinger, CR and iso-conversion methods (OFW and KAS). In each method, Ea was derived from the slope, while A was obtained from the y-intercept of the corresponding equation.

The kinetic parameters were evaluated by plotting $ln\left[\frac{g(\alpha)}{T^2}\right]$, $ln\left(\frac{\beta}{T_m^2}\right)$, $ln\beta$, and $ln\left(\frac{\beta_i}{T_\alpha^2}\right)$ plotted against the inverse of temperature in Kelvin ($1/T$), respectively, for each method for biomass at different heating rates (Lim et al., 2016; Madany et al., 2023).

Thus, the slope line is used to calculate the value of Ea as a function of the conversion rate (α) and heating rate (β).

Although the Kissinger, KAS, and OFW kinetic models are known for their simplicity, they are often criticized for being too general. In contrast, the CR model produces superior qualitative outcomes, but its main drawback is its high complexity.

3. Results and discussions

3.1. Experimental results

3.1.1. Biomass characterization: proximate analysis and ultimate analysis

The proximate and ultimate analysis of PEFB are presented in Table 1 (Lahboubi et al., 2022b). Ultimate analysis of PEFB revealed a high proportion of carbon (40.3 %), followed by oxygen (47 %) and hydrogen (6.4 %). These findings are consistent with those reported in the literature (Sembiring et al., 2015; Fauziyah et al., 2024).

The results of the proximate analysis demonstrated that the proportion of cellulose, hemicelluloses and lignin were found to be 16 %, 9.5 %, and 9.4 % respectively. The results differ slightly from those in the literature, primarily due to the drying time (24 h) and the drying temperature (105 °C), which resulted in a high ash content. For example, Yiin et al., (2018) reported a drying temperature of 80 °C for 18 h, resulting in a hemicellulose content of 26.9 %, a cellulose content of 26.6 %, a lignin content of 25.4 %, and an ash content of 21.1 %. Idris et al., (2021) demonstrated that the application of drying at 100 °C for 12 h resulted in the production of a material comprising 51.2 % cellulose, 20.3 % hemicellulose, 25.4 % lignin, and 3.1 % ash.

3.1.2. Thermogravimetric analysis (TGA)

Fig. 1 shows the TGA (a), the derivative of the thermogravimetric curve DTG (b) and the conversion rate (c) curves of the pyrolysis of PEFB as a function of temperature. The DTG curves fitted with nonlinear least squares method for PEFB at 50 °C/min are presented in Fig. S1. The biomass conversion rate noted α is calculated using Eq. (3).

The pyrolysis process of PEFB exhibits three distinct stages of weight loss at different heating rates, which is consistent with previous studies on the pyrolysis of other biomass materials (Chong et al., 2020; Patrick et al., 2020; Fauziyah et al., 2024). This suggests a common pattern in the pyrolysis behavior of such materials. The first stage, which occurs at around 100 °C, corresponds to the evaporation of water and light components from PEFB, resulting in a 5.5 % mass loss and a conversion rate between 0 and 0.1. The second stage involves the degradation of cellulose and hemicellulose. The first peak of hemicellulose degradation occurs at a temperature below 200 °C, due to its low-level polymerization structure, while the second peak varies depending on the heating rate, with a conversion rate between 0.33 and 0.36 for the different heating rates. Specifically, at a heating rate of 10 °C/min, the maximum peak temperature is around 287 °C; at 30 °C/min, it is 302 °C; and at 50 °C/min, it is 314 °C. The degradation of cellulose varies with the heating rate, as evidenced by the highest peak. The conversion rates of the maximum degradation of cellulose range from 0.67 to 0.69 for the different heating rates. It should be noted that this minimal variation in conversion rates between the beginning and end of the degradation process, with rates of 0.33–0.36 and 0.67 and 0.69, is due to the effect of the reduced thermal inertia of the PEFB. This increases the degradation of the cellulose when more heat is provided. As the heating rate increases, the DTG peak also increases. For instance, at a heating rate of 10 °C/min, the maximum DTG is at 335 °C; at 30 °C/min, it rises to 349 °C; and at 50 °C/min, it reaches 361 °C. Cellulose decomposition involves depolymerization, dehydration, decarboxylation, and aromatization. The third stage, which is the longest decomposition stage, ranges from 250 to 600 °C. This slow degradation of lignin is due to its complex structure and thermal stability, resulting in residual masses varying between 19 % and 24 % for all heating rates.

3.1.3. Visualization of empty fruit bunch through hot stage microscopy

The thermal characteristics of PEFB can be analyzed through shrinkage measurements using a hot stage microscope. This technique demonstrates the gradual evolution of PEFB during thermal decomposition, providing valuable insights into its behavior and color changes throughout this process. Images in Fig. 2 (a, b) depict a PEFB sample before and after pyrolysis. The process starts with a slight shrinkage at 178 °C, followed by the onset of darkness around 230 °C. As the temperature increases, a notable shrinkage occurs around 300 °C, indicating significant structural changes within PEFB.

Finally, the sample reaches complete darkness at 366 °C, signifying the completion of the carbonization reaction, while the PEFB continues to shrink. In Fig. 2, S ratio, DTG, and conversion rate α are plotted as a

Table 1
Proximate and ultimate analysis of PEFB.

Ultimate Analysis (%)				Proximate Analysis (%)			
C	H	N	O	Cellulose	Hemicellulose	Lignin	Extractives and Ash
40.3	6.4	1.1	47	16	9.5	9.4	>32

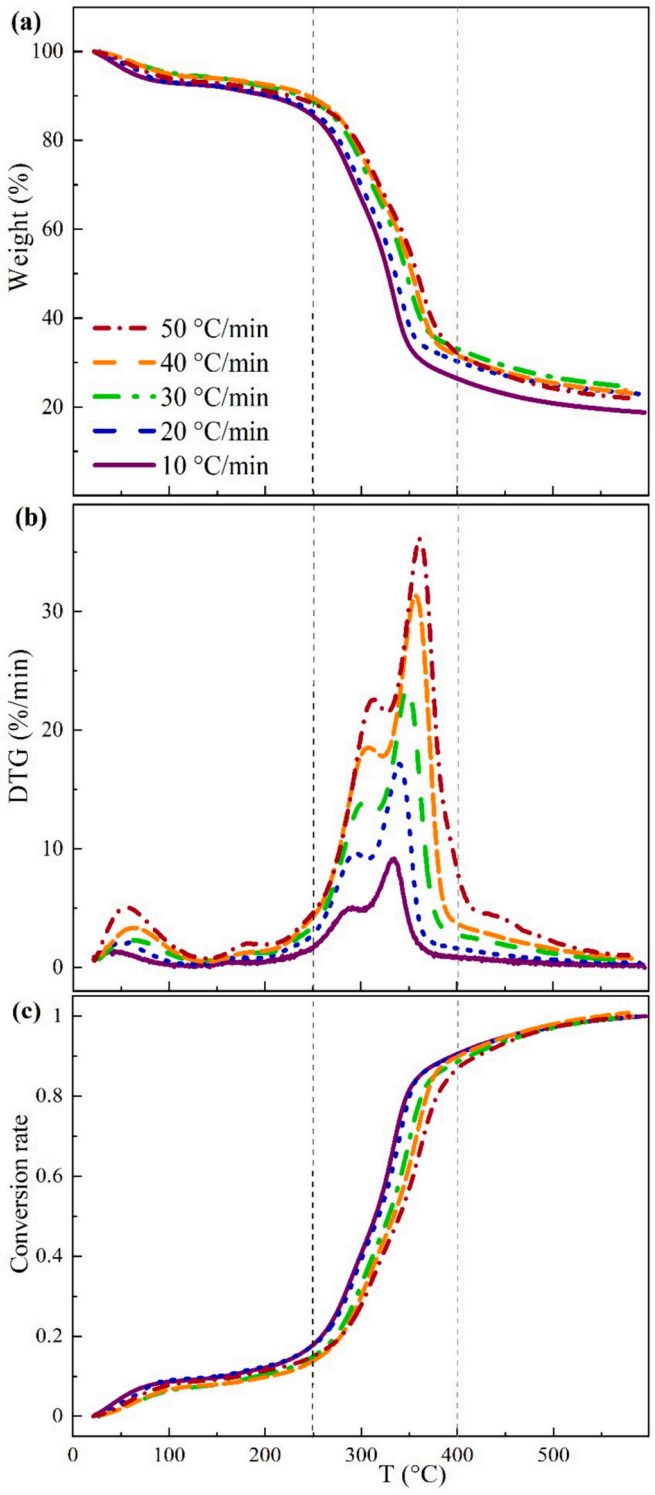

Fig. 1. Thermal evolution of (a) weight, (b) DTG and (c) conversion rate at heating rates 10, 20, 30, 40, and 50 °C/min for PEFB.

function of temperature. The curves of conversion rate and *S* present the same behavior. The conversion rate α, which ranges from 0.2 to 0.8, coincides with the beginning of biomass shrinkage, indicating that significant physical and chemical transformations (Dhahak et al., 2024) occur within this range of conversion rate. Significantly, the onset of increased shrinkage corresponds with the maximum decomposition of the second peak of hemicellulose at around 300 °C. This synchronization highlights a crucial stage where significant changes occur, marking an important point in the conversion process.

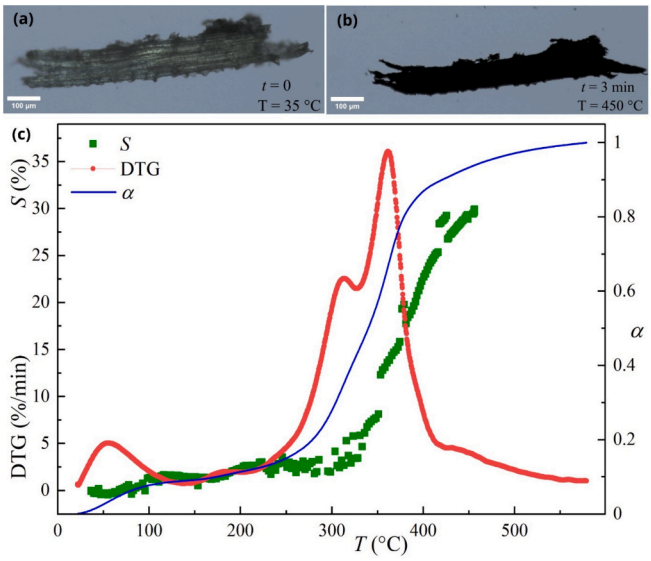

Fig. 2. Images of PEFB before (a) and after (b) pyrolysis in the hot stage microscope at 150 °C/min. (c) DTG and conversion factor as a function of temperature at 50 °C/min combined with shrinkage ratio from image analysis.

3.2. Evaluation and discussion of the kinetic parameters of PEFB

3.2.1. Model-free kinetics: coats and Redfern (CR) approximation

The Coats and Redfern model was used to study the pyrolysis of PEFB at different chemical reaction orders ($n = 1$, $n = 1.5$, and $n = 2$), using the linear regression analysis presented in Fig. 3 and Table S1 for each case. Table S3 in the supplementary material presents data for the activation energy, pre-exponential factor and R^2 correlation coefficient for different heating rates and conversion rate ranges from the analysis of these linear regressions.

When examining chemical reaction models of different orders ($n = 1$, 1.5, and 2), Coast and Redfern's model was found to be inadequate for the full range of conversion rates between 0 and 1. The model CR produced the correlations coefficient and average activation energies of $E_a = 16.74$ kJ/mol ($R^2 = 0.8487$) and $A = 4.406\ min^{-1}$ for $n = 1$, 22.95 kJ/mol ($R^2 = 0.8822$) and $A = 651.33\ min^{-1}$ for $n = 1.5$, and $E_a = 28.81$ kJ/mol ($R^2 = 0.7656$) and $A = 270.29\ min^{-1}$ for $n = 2$, which are considered too low. Despite its simplicity, this model provides valuable insights into the evolving reaction mechanisms during pyrolysis at different conversion rates.

In the context of conversion rates ranging from 0 to 0.2, characterized by low activation energies and pre-exponential factors, the observed values average at $E_a = 8.45$ kJ/mol with $A \leq 0.21\ min^{-1}$ for $n = 1$, $E_a = -2.59$ kJ/mol with $A \leq -0.054\ min^{-1}$ for $n = 1.5$, and $E_a = 9.90$ kJ/mol with $A \leq 1.61\ min^{-1}$ for $n = 2$. This behavior can be attributed to the absence of significant degradation in this phase, which is primarily associated with dehydration processes.

In the conversion rate range of 0.8 to 1, particularly for reaction orders $n = 1.5$ and $n = 2$, there is a notable increase in activation energies. Specifically, there is an increase to $E_a = 118.37$ kJ/mol with an average R^2 of 0.8073 and $A = 5.43 \times 10^{11}\ min^{-1}$ for $n = 1.5$, and an increase to $E_a = 78.08$ kJ/mol with an average R^2 of 0.8084 and $A = 2.04 \times 10^{7}\ min^{-1}$ for $n = 2$ in this range. These increased activation energies are associated with the degradation of lignin, a compound known for its complex structure that requires higher temperatures for efficient breakdown.

It should be noted that, at order $n = 1$, the model used is unable to accurately evaluate the lignin degradation process. This results in a

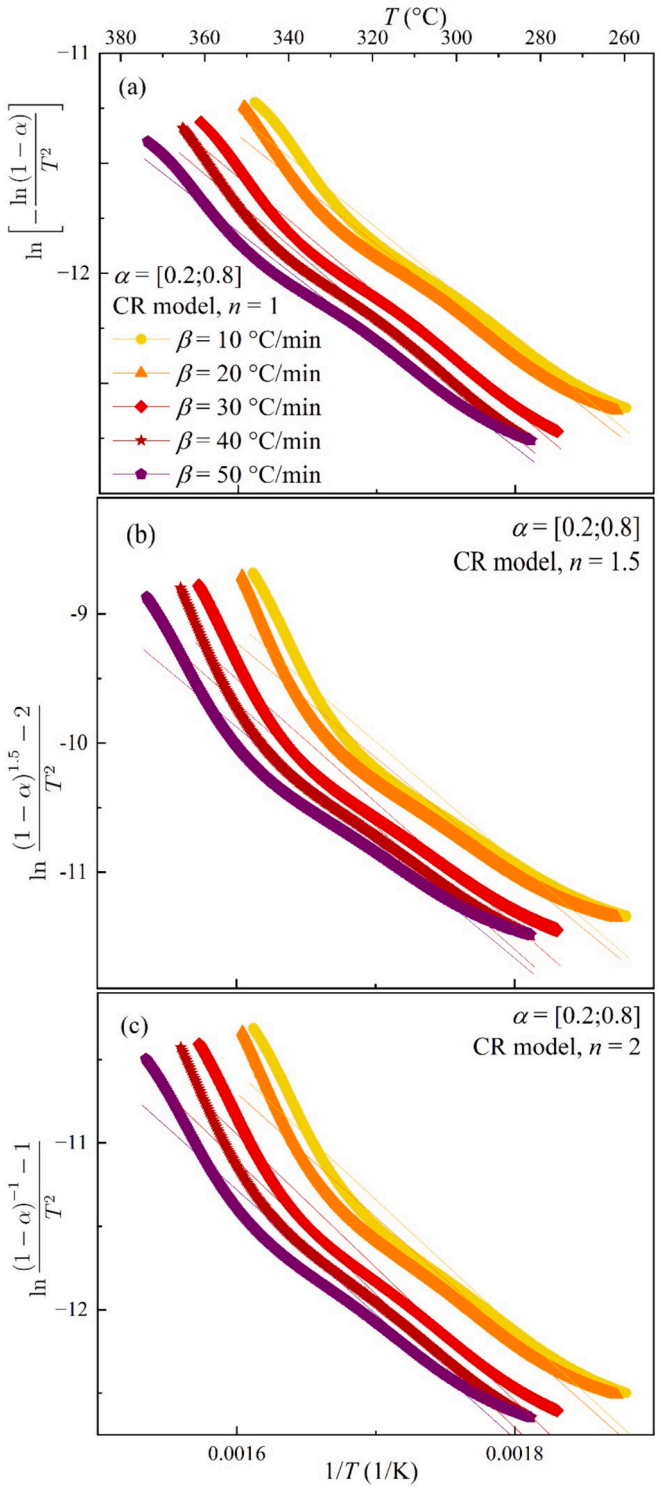

Fig. 3. Coats Redfern regression line reference for conversion rate range 0.2 ≤ α ≤ 0.8 at different reaction order, (a) n = 1, (b) n = 1, and (c) n = 2.

decrease in activation energy to an average of E_a = 9.84 kJ/mol with R^2 of 0.8689.

This study focuses on the interval where mass degradation exceeds 60 % to refine the CR and KAS models. The aim is to enhance the correlation by restricting the study area, ensuring a robust correlation coefficient of $R^2 \geq 0.9$. The findings reveal a significant rise in activation energy within the conversion rate range of 0.2 ≤ α ≤ 0.8. Additionally, exceptional R^2 correlation coefficients exceeding 0.9877 were observed across all five heating rates. Table 2 presents the temperature ranges for this conversion rate range at different heating rates.

Using the first-order chemical reaction model (n = 1), the range of activation energies is determined between 49.121 and 52.599 kJ/mol for 0.2 ≤ α ≤ 0.8 with a robust coefficient R^2 between 0.9877 and 0.9923. These findings are in line with previous research, as demonstrated by Soon et al., (2016). They found that E_a for palm leaves varied between 29.05 and 64.60 kJ/mol for heating rates ranging from 10 to 50 °C/min. The pre-exponential factor, in this study, increases with higher heating rates, ranging from 4.6 ×10^3 to 8.86 ×10^3 min^{-1}, between 10 and 50 °C/min, respectively. The CR model easily overcomes the complexity of the reaction with lower pre-exponential factors $A < 10^8$ because it takes into account, in the formula, small variations in the conversion rate. It also shows a low molecular collision during the reaction taken at each small variation in the conversion rate.

In the chemical reaction model at order n = 1.5, within the range 0.2 ≤ α ≤ 0.8, a notable increase in activation energies is observed, varying from 58.395 ≤ E_a ≤ 63.368 kJ/mol, accompanied by a strong correlation coefficient ranging between 0.9682 ≤ R^2 ≤ 0.9826. The associated pre-exponential factor falls within 3.13 ×10^5 ≤ A ≤ 1.22 ×10^6 min^{-1}.

The CR model of order n = 1.5 emerges as the most suitable, providing a comprehensive explanation of the reaction mechanism. The conversion rate between 0 ≤ α ≤ 0.2, with the E_a being low, between −4.076 ≤ E_a ≤ 3.995 kJ/mol, shows the absence of hemicellulose and cellulose degradation at this phase, and confirms that there was just dehydration. The model also confirms that hemicellulose and cellulose degradation actually take place at phase 2 for 0.2 ≤ α ≤ 0.8. It finally shows that lignin requires a high activation energy and is actually totally degraded during this phase, hence an E_a between 101.44 ≤ E_a ≤ 134.52 kJ/mol.

The model of the chemical reaction of the second order (n = 2) shows, unlike the order n = 1.5, that part of the line is degraded in phase 2 for the conversion rate 0.2 ≤ α ≤ 0.8, which implies an increase in the activation energy in this phase between 65.627 ≤ E_a ≤ 75.045 kJ/mol with an R^2 of 0.963 ≤ R^2 ≤ 0.9725 and a pre-exponential factor of 8.49×10^5 ≤ A ≤ 3.14×10^6 min^{-1}. As part of the lignin is degraded in phase 2, we see a drop in the activation energy. Therefore, for conversion rates, $\alpha \geq 0.9$. Table 3 compares the E_a in the literature with the E_a in this present study. (See Table 4.)

3.2.2. *Kissinger method*

The Kissinger method provides a unique value for the activation energy as it is obtained at the point of the maximum derivative of the thermogravimetric (DTG) curve, which represents the overall reaction process and is consistent across the five heating rates. However, it is important to note that the Kissinger method may not fully elucidate the complexity of the reaction mechanism (Colpani et al., 2022).

The temperature peaks were identified by analyzing the DTG peaks shown in Fig. 1(b). Table 3 displays the regression equations, correlation coefficients (R^2), activation energies (E_a), and pre-exponential factors (A). These values were calculated using the slope of −18,199.2 and y-intercept of 19.689 of the regression lines in Fig. 4. The Kissinger method was used to determine an activation energy of E_a = 151.31 kJ/mol and a pre-exponential factor of A = 1.85E+15 min^{-1}, with a fairly robust correlation coefficient of R2 = 0.966, showing that the Kissinger

Table 2
Range of conversion rate used in the study.

β (°C/min)	***T*** **(°C)** α = [0.2; 0.8]
10	259; 347
20	263; 350
30	273; 363
40	279; 368
50	279; 379

Table 3
Activation energy from the present study and comparison with literature.

Coats and Redfern (CR) Approximation				
Feedstocks	E_a (kJ/mol) $n = 1$	E_a (kJ/mol) $n = 1.5$	E_a (kJ/mol) $n = 2$	References
PEFB ($0.2 \leq \alpha \leq 0.8$) $\beta = \{10; 20; 30; 40; 50\ °C/min\}$	[46.27; 52.569]	[53.941; 63.352]	[65.627; 75.034]	This study
Date palm fiber ($0.2 \leq \alpha \leq 0.8$) $\beta = \{10; 20; 30; 40\ °C/min\}$	58.07	78.72	98.93	(Raza et al., 2021)
PEFB ($0 \leq \alpha \leq 1$) $\beta = \{5; 10; 20\ °C/min\}$	17.24	40.2	60.41	(Wang et al., 2022)
PEFB ($0.2 \leq \alpha \leq 0.8$) $\beta = \{5; 10; 15\ °C/min\}$	[30.15; 31.44]	–	[50.59; 51.26]	(Sidek et al., 2022)
Kissinger Method				
Feedstocks	Catalysts	E_a (kJ/mol)		References
PEFB	–	151.31		This study
Rice husk	Zeolith	153.10		(Loy et al., 2019)
	Nickel	199.9		
beechwood and flax shives	–	~183.81		(Abdelouahed et al., 2017)
Ozawa- Flynn-Wall method (OFW)				
PEFB	–	153.69		This study
PEFB	-	65,12-122,83		(Fauziyah et al., 2024)
	Clam shell	66.25–119.79		
Tithonia diversifolia	Zeolite (HZSM-5, Co/ZSM-5 and Ni/ZSM-5)	105–151.4		(Bhuyan et al., 2024)

Table 4
Kinetic parameters of PEFB by iso-conversional methods KAS and OFW.

	Kissinger Method			OFW Method		
	E_a (kJ/mol)	A	R^2	E_a (kJ/mol)	A	R^2
T_{max} du DTG	151.31	1.85E+15	0.9669	153.69	6.23 E+21	0.971
Alpha (α)	KAS iso-conversion			OFW Method isoconversion		
0.2	125.603	1.29 E+12	0.9102	141.522	4.24 E+21	0.8804
0.3	147.744	1.84 E+13	0.9101	162.901	2.36 E+23	0.9203
0.4	156.806	6.72 E+13	0.871	165.004	1.90 E+23	0.9117
0.5	163.225	1.28 E+14	0.851	163.28	6.49 E+22	0.9161
0.6	157.854	2.77 E+13	0.8489	159.319	1.79 E+22	0.9249
0.7	157.28	1.92 E+13	0.8577	155.682	6.47 E+21	0.9239
0.8	186.014	3.66 E+15	0.7348	147.167	8.53 E+20	0.8849
0.9	–	–	–	161.343	1.98 E+21	0.6091
Means	156.360	5.60 E+14	0.854814	157.027	6.53 E+22	0.871

model fits well with the devolatization of PEFB. The value of the

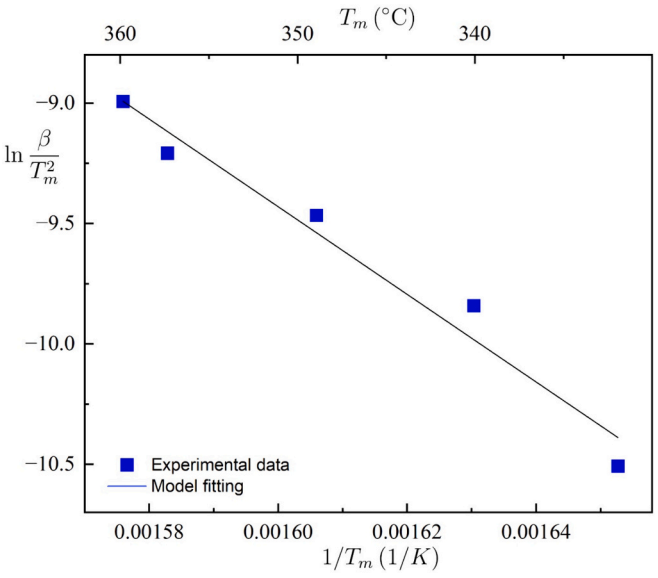

Fig. 4. Kissinger plot of PEFB.

activation energy is close to the results of Mohamed et al., (2020) work, which found $E_a = 167$ kJ/mol without the addition of a catalyst, as in this study, at a heating rate of between 10 and 40 °C/min. This seems to indicate that heating to 50 °C/min slightly reduced the activation energy from 167 to 151 kJ/mol.

The higher pre-exponential factor A, of the order of 10 E+15 above the average of 10 E+14, indicates that PEFB has a complex composition that requires different levels of energy at different stages of thermal degradation, as will be elucidated by the KAS and OFW isoconversion methods. It also reflects higher molecular collisions (Yuan et al., 2017; Chong et al., 2019).

The activation energy values obtained using the Kissinger method are consistent with those obtained by the OFW and KAS methods, which are 156 and 157 kJ/mol, respectively. The pre-exponential factor value is also within the expected range.

3.2.3. KAS method

Table S4 summarizes the activation energies, pre-exponential factors, and correlation coefficients for different conversion rate ranges and heating rates evaluated using the KAS method.

This analysis reveals several very strong overall correlations with the experimental data, with R^2 values >0.98 for all conversion rate ranges.

Additionally, the activation energy shows a slight increase with increasing heating rate, particularly in the conversion rate range of $0.2 \leq \alpha \leq 0.8$. This range is associated with the degradation of hemicellulose and cellulose, where the activation energy falls between $E_a = 9.547$ and $E_a = 9.973$ kJ/mol for all five heating rates. The R^2 values in this range are exceptionally high, exceeding 0.9995, and the pre-exponential coefficient A below 3.59×10^{-2} min^{-1}. Despite the strong correlation, the low activation energies suggest that the generalized KAS model may not accurately describe the data across the entire range of conversion rates. In order to overcome these limitations and provide a more comprehensive kinetic analysis, it was decided to plot isoconversion curves, thus ensuring objectivity and precision in the analysis (Sheng Yong et al., 2023).

3.2.4. Iso-conversional models: Kissinger–Akahira–Sunose method (KAS) and Ozawa- Flynn-Wall method (OFW)

Table 3 presents the activation energies, pre-exponential factors, and correlation coefficients at various conversion rates, by fixing a conversion rate. Fig. 5 shows the linear regression lines derived from the data, and table S2 presents the linear regression equation, providing a visual

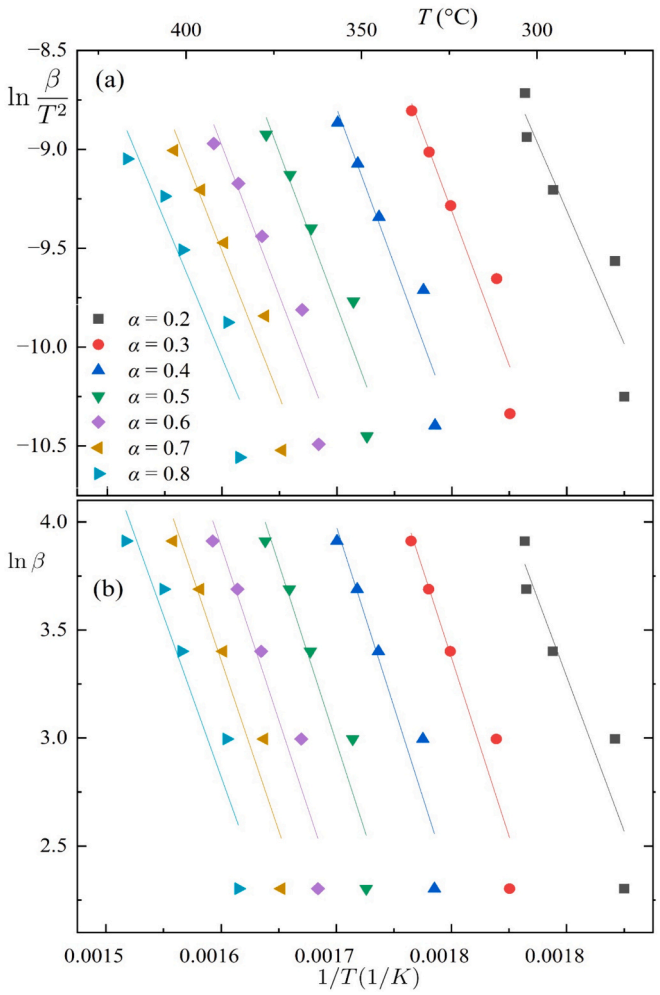

Fig. 5. (a) KAS and (b) OFW plot of PEFB for different values of conversion rate.

representation of the relationship between the kinetic parameters and conversion rates. (See Fig. 6.)

At conversion rates of 0.1 and 0.9, we obtained low E_a values of around $E_a = 7.27$ kJ/mol with poor R^2 values of around 0.066, which shows that there is no degradation of the material at these phases.

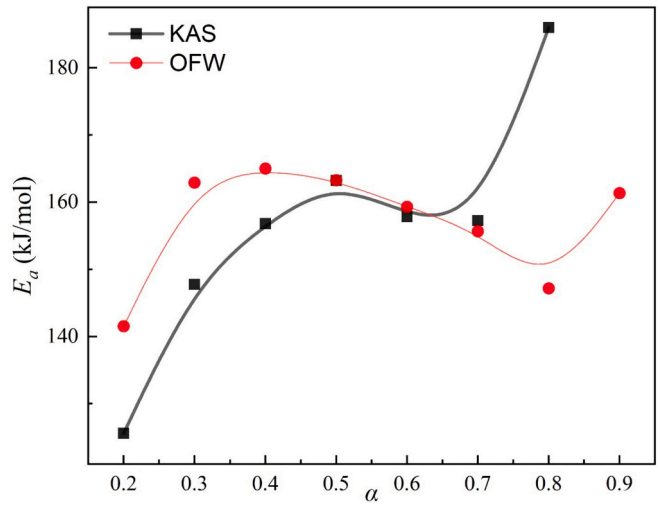

Fig. 6. Activation energy of PEFB at different conversion rates from KAS and OFW models.

Furthermore, as the degree of conversion increases, the activation energy also rises, as demonstrated by the findings of Wang et al., (2022). In fact, materials that have been exposed to high temperatures usually require more energy to be released. Therefore, the higher conversion levels require increased activation energy, indicating a more complex or energy-intensive process. This process may involve the breaking and formation of new chemical bonds or structural rearrangements within the material (Soltani et al., 2023).

Additionally, the activation energies calculated for PEFB using the OFW and KAS models remain relatively constant within the conversion range of $0.2 \leq \alpha \leq 0.8$. For the KAS model, the activation energy values fall within the range of $E_a = 126$ and 186 kJ/mol, while for the OFW model, the range is between $E_a = 142$ and 165 kJ/mol. Fauziyah et al., (2024), who studied PEFB at lower heating rates of 5, 10, and 20 °C/mol, and found that the OFW and KAS method yielded lower activation energies, with values ranging from 65.12 to 122.83 kJ/mol and 54.42 to 102.65 kJ/mol, respectively. While Mohamed et al., (2020) employed a heating rate of 40 °C/min with the OFW model, the resulting activation energy was found to be consistent with that identified in this research, with a value of Ea = 177.68 kJ/mol. Thus, it can be concluded that an increase in the heating rate will result in an elevated activation energy. The pre-exponential factor demonstrates a global increase in value, with a range of 1.29×10^{12} to 3.65×10^{15} min^{-1} for the KAS model and 8.53×10^{20} to 2.36×10^{22} min^{-1} for the OFW model. It is notable that the KAS and OFW models yield particularly high A values in excess of 10E+20. It is evident that PEFB is capable of incorporating a multitude of complex pyrolysis reaction processes across a range of conversion rates. R^2 values also consistently increase, falling within the ranges of $0.7348 \leq R^2 \leq 0.9102$ for the KAS model and $0.8804 \leq R^2 \leq 0.9203$ for the OFW.

Interestingly, the activation energy increases considerably as the degree of conversion reaches higher levels. For KAS, the activation energy reaches up to 186.014 kJ/mol at 80 % conversion, while for OFW, it reaches 161.346 kJ/mol at 90 % conversion (as shown in Fig. 5). This increase in activation energy may be related to the decomposition of lignin, which contains stiffer carbon-carbon bonds that require more energy to be cleaved (Wang et al., 2017).

Fig. 5 shows a slight decrease in activation energy between the conversion rates of 0.5 and 0.6. This may be due to the completion of cellulose degradation just before the onset of lignin degradation. Activation energy represents the minimum energy required for a reaction to occur, and a decrease in E_a suggests that less external energy is needed to overcome the energy barrier, allowing the pyrolysis process to proceed more readily (Wang et al., 2017; Agrizzi et al., 2024).

It should be noted that the decomposition of cellulose occurs in multiple stages, which may explain the decrease in activation energy after a peak at 0.5 conversion rate. Chong et al., (2019), suggest that the decomposition of cellulose at lower temperatures involves at least three distinct stages, each with one or more reactions. The first stage is an endothermic process at around 220 °C. This leads to the formation of 'anhydrocellulose' by intermolecular dehydration. The second reaction takes place at around 280 °C. This is more endothermic than the first reaction and results in the formation of levoglucosan, the primary tar compound. The mechanism for the formation of levoglucosan has been established as a depolymerization reaction of 1,4-anhydro-α-D-glucopyranose (Richter and Rein, 2020).

3.2.5. Comparison of the different mathematical models studied for different heating rates

The analysis of the three models studied in this work, within the conversion rate range of $0.2 \leq \alpha \leq 0.8$, is presented in Table S3. The CR model for the first model ($n = 1$) does not achieve high accuracy due to the low activation energies and pre-exponential factors. This is because these values are evaluated solely based on the reaction rate, which is a function of the concentration of a single component (cellulose,

hemicellulose, or lignin). However, the accuracy of the reaction mechanism improves for $n \neq 1$ (1.5 or 2), as the reaction rate becomes proportional either to the square of the concentration of one component or to the concentration of the interaction of at least two components. The order $n \neq 1$ aligns the results of the CR model with the KAS and OFW models, which yield higher values. Therefore, the activation energies range from 60 to 134 kJ/mol, which is similar to the averages obtained with the KAS and OFW models, which are 156 and 157 kJ/mol, respectively. In addition, the CR model shows that the activation energy of the reaction is not significantly affected by the variation in heating rate. However, it does increase the number of molecular collisions, as indicated by the pre-exponential factor. All three models (CR, KAS, and OFW) consistently show that the activation energy increases as the temperature increases, corresponding to the degradation of the more thermally stable components. This suggests that the three models are complementary and jointly suitable for describing the pyrolysis of PEFB.

4. Perspectives and challenges

The study yielded encouraging findings regarding the potential of PEFB to be converted by pyrolysis for bioenergy. The activation energy of PEFB is low, averaging no >153 kJ/mol for the four kinetic models, even in the absence of a catalyst and without delignifying the raw material through pre-treatment. It can therefore be employed for cost-effective industrial production that is less energy-intensive and environmentally friendly (Junsittiwate et al., 2022).

Nevertheless, it would be enlightening to observe the collective impact of delignification and the incorporation of catalysts, such as zeolite, on the kinetics of PEFB pyrolysis. As demonstrated by Loy et al., (2019), the addition of zeolite can reduce the pyrolysis activation energy of a feedstock to a value exceeding 30 kJ/mol. Similarly, Idris et al., (2021) illustrates that the delignification process can also result in a reduction of this activation energy to a value exceeding 40 kJ/mol.

5. Conclusions

This study investigated the behavior of PEFB constituents during pyrolysis, as indicated by kinetics, TGA, and shrinkage analysis. The results provide insights into the optimal degradation temperature and the devolatilization temperature range of components of PEFB, namely hemicellulose, cellulose, and lignin. The Coast-Redfern model was found to be a good fit for the kinetic reaction at orders $n = 1.5$ and 2. The Kissinger, KAS and OFW models were used to evaluate each stage, providing a general view of the reaction. The four models exhibited relatively low average activation energies, with values ranging from 70 to 151 kJ/mol. This indicates that PEFB can be employed for the production of biofuels with minimal energy requirements and that it is environmentally friendly.

Conflict of interest declaration

All authors agree that author list is correct in its content and order and that no modification to the author list can be made without the formal approval of the Editor-in-Chief, and all authors accept that the Editor-in-Chief's decisions over acceptance or rejection or in the event of any breach of the Principles of Ethical Publishing in the Journal of *Bioresource Technology reports* being discovered of retraction are final. No additional authors will be added post submission, unless editors receive agreement from all authors and detailed information is supplied as to why the author list should be amended.

CRediT authorship contribution statement

Casimir Kalibé Fanezouné: Writing – review & editing, Writing – original draft, Visualization, Resources, Methodology, Investigation, Formal analysis, Conceptualization. **Asma Dhahak:** Writing – review & editing, Writing – original draft, Methodology. **Jorge Peixinho:** Writing – review & editing, Validation, Methodology. **Hassan El Bari:** Visualization, Validation, Supervision, Project administration, Methodology, Conceptualization.

Declaration of competing interest

The authors declare that they have no known competing financial interests or personal relationships that could have appeared to influence the work reported in this paper.

Data availability

Data will be made available on request.

Acknowledgment

This publication is part of the funding Project titled "Sustainable biomass conversion into bioenergy through pyrolysis" (PyroBioFuel) - LEAP-RE (Europe-Africa Renewable Energy). The authors acknowledge the financial support of the Agence Nationale de la Recherche (ANR) through the PyroBioFuel project funded by the European Union's Horizon 2020 Research and Innovation Program under Grant Agreement 963530.

References

Agoudjil, B., Benchabane, A., Boudenne, A., Ibos, L., Fois, M., 2011. Renewable materials to reduce building heat loss: Characterization of date palm wood. Energ. Buildings 43, 491–497. https://doi.org/10.1016/j.enbuild.2010.10.014.

Agrizzi, T., Oliveira, M.A., Faria, E.V., Santos, K.G., Xavier, T.P., Lira, T.S., 2024. Assessing coconut shell pyrolysis: Biomass characterization, activation energy estimation, and statistical analysis of operating conditions. Bioresource Technology Reports 26, 101831. https://doi.org/10.1016/j.biteb.2024.101831.

Ahmad, M.S., Mehmood, M.A., Al Ayed, O.S., Ye, G., Luo, H., Ibrahim, M., Rashid, U., Arbi Nehdi, I., Qadir, G., 2017. Analyses cinétiques et comportement pyrolytique de l'herbe Para (*Urochloa mutica*) pour son potentiel bioénergétique. Bioresour. Technol. 224, 708–713. https://doi.org/10.1016/j.biortech.2016.10.090.

Akinnawo, O.O., Nurhafizah, M.D., Abdullah, N., 2023. Pyrolysis Kinetic Study of the Thermal Degradation of Pre-Treated Empty Fruit Bunches. Proceedings, Materials Today. https://doi.org/10.1016/j.matpr.2023.03.512.

Al-Maari, M.A., Ahmad, M.A., Din, A.T.M., Hassan, H., Alsobaai, A.M., 2021. Co-pyrolysis of oil palm empty fruit bunch and oil palm frond with low-density polyethylene and polypro- pylene for bio-oil production. Arab. J. Chem. 14, 103282 https://doi.org/10.1016/j.arabjc.2021.103282.

Anca-Couce, A., Mehrabian Bardar, R., Scharler, R., Obernberger, I., 2014. Kinetic scheme of biomass pyrolysis considering secondary charring reactions. Energ. Conver. Manage. 87, 687–696. https://doi.org/10.1016/j.enconman.2014.07.061.

Beniche, I., Bari, H.E., Siles, J.A., Chica, A.F., Martín, M.Á., 2021. Methane production by anaerobic co-digestion of mixed agricultural waste: cabbage and cauliflower. Environ. Technol. 42, 4550–4558. https://doi.org/10.1080/09593330.2020.1770341.

Bensidhom, G., Ben Hassen-Trabelsi, A., Alper, K., Sghairoun, M., Zaafouri, K., Trabelsi, I., 2018. Pyrolysis of date palm waste in a fixed-bed reactor: Characterization of pyrolytic products. Bioresour. Technol. 247, 363–369. https://doi.org/10.1016/j.biortech.2017.09.066.

Blaine, R.L., Kissinger, H.E., 2012. Homer Kissinger and the Kissinger equation. Thermochim. Acta 540, 1–6. https://doi.org/10.1016/j.tca.2012.04.008.

Boukaous, N., Abdelouahed, L., Chikhi, M., Mohabeer, C., Meniai, A.H., Taouk, B., 2021. Investigations on Mediterranean biomass pyrolysis ability by thermogravimetric analyses: thermal behaviour and sensitivity of kinetic parameters. C. R. Chim. 23, 623–634. https://doi.org/10.5802/crchim.56.

Chong, C.T., Mong, G.R., Ng, J.-H., Chong, W.W.F., Ani, F.N., Lam, S.S., Ong, H.C., 2019. Pyrolysis characteristics and kinetic studies of horse manure using thermogravimetric analysis. Energ. Conver. Manage. 180, 1260–1267. https://doi.org/10.1016/j.enconman.2018.11.071.

Chong, Y.Y., Ng, H.K., Lee, L.Y., Gan, S., Thangalazhy-Gopakumar, S., 2020. Kinetics and mecha- nisms for catalytic pyrolysis of empty fruit bunch fibre and cellulose with oxides. SN Appl. Sci. 2, 1464. https://doi.org/10.1007/s42452-020-03249-1.

Colpani, D., Santos, V.O., Araujo, R.O., Lima, V.M.R., Tenório, J.A.S., Coleti, J., Chaar, J. S., de Souza, L.K.C., 2022. Bioenergy potential analysis of Brazil nut biomass

residues through pyrolysis: Gas emission, kinetics, and thermodynamic parameters. Cleaner Chemical Engineering 1, 100002. https://doi.org/10.1016/j.clce.2022.100002.
Dhahak, A., Cézard, L., Baumberger, S., Peixinho, J., 2024. Kinetic, products and shrinkage for the pyrolysis of flax fibers. J. Anal. Appl. Pyrolysis 180, 106538. https://doi.org/10.1016/j.jaap.2024.106538.
El Bari, H., Fanezoune, C.K., Dorneanu, B., Arellano-Garcia, H., Majozi, T., Elhenawy, Y., Bayssi, O., Hirt, A., Peixinho, J., Dhahak, A., Gadalla, M.A., Khashaba, N.H., Ashour, F.H., 2024. Catalytic fast pyrolysis of lignocellulosic biomass: recent advances and comprehensive overview. J. Anal. Appl. Pyrolysis 178, 106390. https://doi.org/10.1016/j.jaap.2024.106390.
El Gnaoui, Y., Frimane, A., Lahboubi, N., Herrmann, C., Barz, M.E.L., Bari, H., 2022. Biological pre-hydrolysis and thermal pretreatment applied for anaerobic digestion improve- ment: Kinetic study and statistical variable selection. Cleaner Waste Systems 2, 100005. https://doi.org/10.1016/j.clwas.2022.100005.
Elsayed, M., Abomohra, A.E.-F., Ai, P., Wang, D., El-Mashad, H.M., Zhang, Y., 2018. Biorefining of rice straw by sequential fermentation and anaerobic digestion for bioethanol and/or biomethane production: Comparison of structural properties and energy output. Bioresour. Technol. 268, 183–189. https://doi.org/10.1016/j.biortech.2018.07.130.
Fauziyah, Aprianti, N., Rozirwan, Yahyah, Dollu, E., Diansyah, G., 2024. Kinetics and thermody- namic parameters of palm empty fruit bunch pyrolysis promoted by calcium-rich wastes from coastal-marine residue. Bioresource Technology Reports 25, 101735. https://doi.org/10.1016/j.biteb.2023.101735.
Ferreira, M.F.P., Oliveira, B.F.H., Pinheiro, W.B.S., Correa, N.F., França, L.F., Ribeiro, N. F.P., 2020. Generation of biofuels by slow pyrolysis of palm empty fruit bunches: Optimi- zation of process variables and characterization of physical-chemical products. Biomass Bioenergy 140, 105707. https://doi.org/10.1016/j.biombioe.2020.105707.
Ghnimi, S., Umer, S., Karim, A., Kamal-Eldin, A., 2017. Fruits de dattes (*Phoenix dactylifera*l.) : Une alimentation sous-utilisée en quête de valorisation industrielle. NFS Journal 6, 1–10. https://doi.org/10.1016/j.nfs.2016.12.001.
Gil, M.V., Casal, D., Pevida, C., Pis, J.J., Rubiera, F., 2010. Thermal behaviour and kinetics of coal/biomass blends during co-combustion. Bioresour. Technol. 101, 5601–5608. https://doi.org/10.1016/j.biortech.2010.02.008.
Habchi, S., Lahboubi, N., Asbik, M., Bari, H.E., 2024. Enhancing biomethane production from food waste using olive pomace hydrochar: an optimization study. Environmental Advances 15, 100477. https://doi.org/10.1016/j.envadv.2023.100477.
Handoko, S., Nurhadi, N., Mujiati, S., Fitriani, R., 2021. Characterization of pyrolysis products of oil palm empty fruit bunch. IOP Conf. Ser.: Earth Environ. Sci. 749, 012041 https://doi.org/10.1088/1755-1315/749/1/012041.
Idris, R., Chong, W.W.F., Ali, A., Idris, S., Hasan, M.F., Ani, F.N., Chong, C.T., 2021. Phenol-rich bio-oil derivation via microwave-induced fast pyrolysis of oil palm empty fruit bunch with activated carbon. Environmental Technology & Innovation 21, 101291. https://doi.org/10.1016/j.eti.2020.101291.
Junsittiwate, R., Srinophakun, T.R., Sukpancharoen, S., 2022. Techno-economic, environmental, and heat integration of palm empty fruit bunch upgrading for power generation. Energy Sustain. Dev. 66, 140–150. https://doi.org/10.1016/j.esd.2021.12.001.
Ke, J., Singh, D., Yang, X., Chen, S., 2011. Caractérisation thermique de la modification de la lignine des résineux par le termite *Coptotermes formosanus* (Shiraki). Biomass and Bioenergy, PROCEEDINGS OF A WORKSHOP OF IEA BIOENERGY TASK 31 ON 'SUSTAINABLE FORESTRY SYSTEMS FOR BIOENERGY: INTEGRATION. INNOVATION AND INFORMATION' 35, 3617–3626. https://doi.org/10.1016/j.biombioe.2011.05.010.
Lahboubi, N., Karouach, F., Bakraoui, M., El Gnaoui, Y., Essamri, A., El Bari, H., 2022a. Effect of Alkali-NaOH Pretreatment on methane production from Anaerobic Digestion of date Palm Waste. Ecol. Eng. Environ. Technol. 23, 78–89. https://doi.org/10.12912/27197050/144846.
Lahboubi, N., Kerrou, O., Karouach, F., Bakraoui, M., Schüch, A., Schmedemann, K., Stinner, W., El Bari, H., Essamri, A., 2022b. Methane production from mesophilic fed-batch anaerobic digestion of empty fruit bunch of palm tree. Biomass Conv. Bioref. 12, 3751–3760. https://doi.org/10.1007/s13399-020-00864-1.
Liang, W., Feng, Y., Wang, K., Wang, C., Yang, H., 2024. Investigation on pyrolysis characte- ristics and kinetics of sewage sludge with different heat-mass transfer rates. Fuel 372, 132192. https://doi.org/10.1016/j.fuel.2024.132192.
Lim, A.C.R., Chin, B.L.F., Jawad, Z.A., Hii, K.L., 2016. Kinetic Analysis of Rice Husk Pyrolysis using Kissinger-Akahira-Sunose (KAS) Method. In: Procedia Engineering, Proceeding of 4th International Conference on Process Engineering and Advanced Materials (ICPEAM 2016) 148, pp. 1247–1251. https://doi.org/10.1016/j.proeng.2016.06.486.
Madany, N., Gadalla, M., Ashour, F.H., Abadir, M., 2023. Investigating the Kinetic Parameters in the thermal Analysis of Jojoba Cake. Egypt. J. Chem. 66, 245–256. https://doi.org/10.21608/ejchem.2022.160576.6924.
Makowska, M., Dziosa, K., 2024. Influence de différentes températures de pyrolyse sur la composition chimique et la structure de type graphite du biochar produit à partir de la biomasse de microalgues vertes *Chlorella sp*. Environmental Technology & Innovation 35, 103667. https://doi.org/10.1016/j.eti.2024.103667.
Matali, S., Abd Rahman, N., Idris, S.S., Yaacob, N., 2020. Dynamic Model-Free and Model-Fitting Kinetic Analysis during Torrefaction of Oil Palm Frond Pellets. Bull. Chem. React. Eng. Catal. 15, 253–263. https://doi.org/10.9767/bcrec.15.1.6985.253-263.
Mohamed, A.R., Zin, A.M., Ahmad Termizi, S.N.A., Sohaimi, K.S.A., Izhar, N.I.I.N., 2020. Kinetics Analysis on Catalytic Pyrolysis of empty Fruit Bunch (EFB) with Copper Oxide Doped Aluminium Oxide (CuO/Al_2O_3) Catalyst. IOP Conf. Ser.: Mater. Sci. Eng. 932, 012010 https://doi.org/10.1088/1757-899X/932/1/012010.
Naqvi, S.R., Tariq, R., Hameed, Z., Ali, I., Naqvi, M., Chen, W.-H., Ceylan, S., Rashid, H., Ahmad, J., Taqvi, S.A., Shahbaz, M., 2019. Pyrolysis of high ash sewage sludge: Kinetics and thermodynamic analysis using Coats-Redfern method. Renew. Energy 131, 854–860. https://doi.org/10.1016/j.renene.2018.07.094.
Nasser, R., Salem, M., Hiziroglu, S., Al-Mefarrej, H., Mohareb, A., Alam, M., Aref, I., 2016. Chemical Analysis of different parts of date Palm (Phoenix dactylifera L.) using Ultimate, Proximate and Thermo-Gravimetric Techniques for Energy Production. Energies 9, 374. https://doi.org/10.3390/en9050374.
Nyakuma, B.B., Ahmad, A., Johari, A., Tuan Abdullah, T.A., Oladokun, O., Aminu, D.Y., 2015. Non-isothermal kinetic analysis of oil palm empty fruit bunch pellets by thermogravimetric analysis. Chem. Eng. Trans. 45, 1327–1332. https://doi.org/10.3303/CET1545222.
Nzihou, A., Stanmore, B., Lyczko, N., Minh, D.P., 2019. The catalytic effect of inherent and adsorbed metals on the fast/flash pyrolysis of biomass: a review. Energy 170, 326–337. https://doi.org/10.1016/j.energy.2018.12.174.
Ouhammou, B., Aggour, M., Frimane, A., Bakraoui, M., El Bari, H., Essamri, A., 2019. A new system design and analysis of a solar bio-digester unit. Energ. Conver. Manage. 198, 111779 https://doi.org/10.1016/j.enconman.2019.111779.
Ouhammou, B., Mohammed, A., Sliman, S., Jamil, A., Mohammed, B., Karouach, F., El Bari, H., Kousksou, T., 2022. Experimental conception and thermo-energetic analysis of a solar biogas production system. Case Studies in Thermal Engineering 30, 101740. https://doi.org/10.1016/j.csite.2021.101740.
Patrick, D.O., Yusup, S., Osman, N.B., Zabiri, H., Uemura, Y., Shahbaz, M., 2020. Thermogra- vimetric Kinetics of Catalytic and Non-Catalytic Pyrolytic Conversion of Palm Kernel Shell with Acid-Treated Coal Bottom Ash. Bioenergy Res. 13, 452–462. https://doi.org/10.1007/s12155-020-10101-2.
Phuakpunk, K., Chalermsinsuwan, B., Assabumrungrat, S., 2020. Comparison of chemical reaction kinetic models for corn cob pyrolysis. Energy Reports, Technologies and Materials for Renewable Energy, Environment and Sustainability 6, 168–178. https://doi.org/10.1016/j.egyr.2020.08.041.
Raza, M., Inayat, A., Ahmed, A., Jamil, F., Ghenai, C., Naqvi, S.R., Shanableh, A., Ayoub, M., Waris, A., Park, Y.-K., 2021. Progress of the Pyrolyzer Reactors and Advanced Techno- logies for Biomass Pyrolysis Processing. Sustainability 13, 11061. https://doi.org/10.3390/su131911061.
Richter, F., Rein, G., 2020. Reduced chemical kinetics for microscale pyrolysis of softwood and hardwood. Bioresour. Technol. 301, 122619 https://doi.org/10.1016/j.biortech.2019.122619.
Rousset, M., 2013. 4. Biomasse: de nombreuses filières pour des enjeux importants. In: Mosseri, R., Jeandel, C. (Eds.), L'énergie à découvert, À découvert. CNRS Éditions, Paris, pp. 143–144. https://doi.org/10.4000/books.editionscnrs.11012.
Sedra, M., 2015. Date Palm Status and Perspective in Morocco. Date Palm Genetic Resources and utilization: volume 1: Africa and the Americas 257–323. doi:https://doi.org/10.1007/978-94-017-9694-1_8.
Sembiring, K.C., Rinaldi, N., Simanungkalit, S.P., 2015. Bio-oil from Fast Pyrolysis of empty Fruit Bunch at various Temperature. Energy Procedia 65, 162–169. https://doi.org/10.1016/j.egypro.2015.01.052.
Sheng Yong, Y., Abdul Rasid, R., Ismail, M., 2023. Evaluation of Oil Palm Waste Mild Pyrolysis Kinetic Parameters. Proceedings, Materials Today. https://doi.org/10.1016/j.matpr.2023.03.228.
Sidek, F.N., Saleh, S., Abdul Samad, N.A.F., 2022. Kinetic parameter estimation for pyrolysis of empty fruit bunch using model-fitting and model-free methods. Materials Today: Proceedings 57, 1241–1247. https://doi.org/10.1016/j.matpr.2021.11.141.
Soltani, I., Berrich, E., Romdhane, M., Fethi, A., 2023. Heating rate and ZSM-5 catalyst effects on date palm (Phœnix dactylifera L.) stones pyrolysis: Thermogravimetric analysis, production and characterization of syngases and bio-oils. J. Energy Inst. 110, 101295 https://doi.org/10.1016/j.joei.2023.101295.
Soon, V.S.Y., Chin, B.L.F., Lim, A.C.R., 2016. Kinetic Study on Pyrolysis of Oil Palm Frond. IOP Conf. Ser.: Mater. Sci. Eng. 121, 012004 https://doi.org/10.1088/1757-899X/121/1/012004.
Sounni, F., Elgnaoui, Y., El Bari, H., Merzouki, M., Benlemlih, M., 2023. Effect of mixture ratio and organic loading rate during anaerobic co-digestion of olive mill wastewater and agro-industrial wastes. Biomass Conv. Bioref. 13, 1223–1229. https://doi.org/10.1007/s13399-021-01463-4.
Strauch, S.M., Wenzel, L.C., Bischoff, A., Dellwig, O., Klein, J., Schüch, A., Wasenitz, B., Palm, H.W., 2018. Commercial African Catfish (Clarias gariepinus) Recirculating Aquaculture Systems: Assessment of Element and Energy Pathways with special Focus on the Phosphorus Cycle. Sustainability 10, 1805. https://doi.org/10.3390/su10061805.
Sutrisno, B., Hidayat, A., 2018. Pyrolysis of palm empty fruit bunch: yields and analysis of bio-oil. MATEC Web Conf. 154, 01036 https://doi.org/10.1051/matecconf/201815401036.
Wang, S., Dai, G., Yang, H., Luo, Z., 2017. Lignocellulosic biomass pyrolysis mechanism: a state-of-the-art review. Prog. Energy Combust. Sci. 62, 33–86. https://doi.org/10.1016/j.pecs.2017.05.004.
Wang, W., Lemaire, R., Bensakhria, A., Luart, D., 2022. Review on the catalytic effects of alkali and alkaline earth metals (AAEMs) including sodium, potassium, calcium and magne- sium on the pyrolysis of lignocellulosic biomass and on the co-pyrolysis of coal with biomass. J. Anal. Appl. Pyrolysis 163, 105479. https://doi.org/10.1016/j.jaap.2022.105479.
Xie, Wenhao, Wen, S., Liu, J., Xie, Wuming, Kuo, J., Lu, X., Sun, S., Chang, K., Buyukada, M., Evrendilek, F., 2018. Comparative thermogravimetric analyses of co-combustion of textile dyeing sludge and sugarcane bagasse in carbon dioxide/oxygen and nitrogen/oxygen atmospheres: thermal conversion characteristics,

kinetics, and thermodynamics. Bioresour. Technol. 255, 88–95. https://doi.org/10.1016/j.biortech.2018.01.110.

Yiin, C.L., Yusup, S., Quitain, A.T., Uemura, Y., Sasaki, M., Kida, T., 2018. Thermogravimetric analysis and kinetic modeling of low-transition-temperature mixtures pretreated oil palm empty fruit bunch for possible maximum yield of pyrolysis oil. Bioresour. Technol. 255, 189–197. https://doi.org/10.1016/j.biortech.2018.01.132.

Yuan, X., He, T., Cao, H., Yuan, Q., 2017. Cattle manure pyrolysis process: Kinetic and thermo- dynamic analysis with isoconversional methods. Renew. Energy 107, 489–496. https://doi.org/10.1016/j.renene.2017.02.026.

Zhong, Y., Liu, F., Huang, G., Zhang, J., Li, C., Ding, Y., 2024. Thermogravimetric experiments based prediction of biomass pyrolysis behavior: a comparison of typical machine learning regression models in Scikit-learn. Mar. Pollut. Bull. 202, 116361 https://doi.org/10.1016/j.marpolbul.2024.116361.